JOURNAL OF AIRCRAFT
Vol. 29, No. 3, May–June 1992

Effects of Higher Harmonic Control on Rotor Performance and Control Loads

Khanh Nguyen*
NASA Ames Research Center, Moffett Field, California 94035
and
Inderjit Chopra†
University of Maryland, College Park, Maryland 20742

An analytical study, based on an advanced higher harmonic control analysis for helicopter rotor systems, is carried out to investigate the potential of higher harmonic control to improve rotor performance. The effects of higher harmonic control on the stall characteristics of rotor and blade pitch-link loads when the system is configured to suppress vibration are also examined. The analysis is based on a finite element method in space and time. A nonlinear time domain unsteady aerodynamic model is used to obtain the blade air loads, and the rotor induced inflow is calculated using a nonuniform inflow model. Correlation of the calculated rotor shaft power with experimental data is fair. For performance improvement on a three-bladed rotor, a 1–3.8% reduction in rotor power is achieved with 2-deg amplitude of 2/rev blade pitch control. For vibratory hub shear suppression, simulated results indicate that higher harmonic control may promote early blade stall. Effects of blade torsion frequencies on higher harmonic control performance are moderate, and torsionally stiff blades require less actuator power than torsionally soft blades.

Introduction

OVER the last decade, flight tests conducted by Hughes Helicopters (presently McDonnell Douglas Helicopter Company),[1] Sikorsky Aircraft,[2] and Aerospatiale[3] have convincingly demonstrated that higher harmonic control (HHC) is one of the most effective systems for helicopter vibration suppression. The success of HHC systems stem from the fact that the vibrations are suppressed at the source—the higher harmonic blade air loads. This is in contrast to the passive vibration control devices such as dynamic absorbers and rotor isolators that suppress vibrations after they has been generated. In an HHC system, the higher harmonic blade pitches are excited by servo-actuators to generate new unsteady air loads, which in combination with the resultant inertial loads, cancel the existing vibratory blade loads that cause airframe vibration.

Since an HHC system works by modifying the air loads on the helicopter rotor, it is not presently clear how the rotor stall characteristics would be affected. In fact, all reported HHC flight tests to date were conducted well within the helicopter flight envelope, where the effects of retreating blade stall and advancing blade compressibility were small. For a helicopter operating near the edge of the flight envelope, the HHC used for vibration suppression may induce a premature onset of blade stall. Since a successful HHC system must operate effectively in severe aerodynamic environments, it is of great interest to investigate the effects of HHC at these flight conditions.

Beside vibration control, HHC has potential to improve rotor performance. An HHC system can be configured to postpone retreating blade stall or to redistribute rotor airloads, resulting in an overall improvement in the rotor aerodynamic efficiency. In fact, HHC has long been proposed as a means of delaying the onset of retreating blade stall. In the 1950s and early 1960s, analytical studies carried out by Stewart,[4] Payne,[5] and Arcidiacono[6] all showed that HHC could effectively delay retreating blade stall and, in effect, raise the forward speed limitation of helicopters. These investigators derived the transfer functions relating the higher harmonic inputs to the change in rotor angle-of-attack distribution. The results of these derivations led them to conclude that the rotor lift could be effectively redistributed, while maintaining trim at a given flight condition, to allow the retreating blade to operate at a lower angle of attack.

In 1961, Bell Helicopter Company[7] carried out an HHC flight test on a UH-1A helicopter. One of the objectives was to investigate the use of HHC to alleviate blade stall. The Bell report noted that when 2/rev (2*P*) blade pitch input was phased to reduce retreating blade stall at 100 kt, no reduction in rotor shaft torque was observed. Further investigation showed that, when the 2*P* blade pitch was applied, there was in fact a drag reduction in the retreating side. However, this reduction was commensurate with an increase in the profile drag in the front and rear portions of the rotor disk, resulting in no net reduction in the rotor shaft power.

Recently, the application of 2*P* blade pitch control to improve rotor performance was investigated independently by Boeing Helicopter Company[8] and Aerospatiale.[9] Both of these investigations were carried out using wind-tunnel simulations of two different scaled models of three-bladed rotors. Note that both experiments used swash-plate oscillation to generate the HHC inputs and that the 2*P* blade pitch excitation is feasible for three-bladed rotors. Results from both tests showed that 2*P* blade pitches, when phased properly, could significantly reduce the rotor shaft power. Boeing results showed that 2*P* blade pitch reduced the rotor shaft torque by 6% at 135 kt and 4% at 160 kt. At both flight test conditions, 2 deg of 2*P* blade pitch amplitude was used, and the higher harmonic blade pitch waveforms for both cases were nose up side-to-side relative to the rotor disk. Results from the Aero-

Presented as Paper 90–1158 at the AIAA/ASME/ASCE/AHS/ASC 31st Structures, Structural Dynamics, and Materials Conference, Long Beach, CA, April 1–4, 1990; received April 2, 1990; revision received Feb. 13, 1991; accepted for publication April 6, 1991.

*Aerospace Engineer, Rotorcraft Aeromechanics Branch. Member AIAA.
†Professor, Department of Aerospace Engineering. Member AIAA.

spatiale wind-tunnel HHC test showed >5% reduction in rotor shaft power at an advance ratio of 0.4. This reduction was achieved with 2.8 deg of 2P blade pitch. The higher harmonic blade pitch waveform, which was nose up in the fore and aft portions of the rotor disk, was different from the results reported by Boeing.

The major objective of this paper is to analyze the feasibility of using HHC to improve the basic rotor performance. The influence of HHC on the stall behavior of rotors when the system is engaged to suppress vibratory hub loads is also examined. Another objective is to study HHC effects on the blade pitch-link loads, which directly correspond to the control system loads. The increase in blade pitch-link loads, typically associated with the applied HHC inputs, can be significant, especially at the high-speed, high-thrust flight regimes. This particular problem has a practical significance since the pitch-link loads directly influence the actuator power requirement of both the HHC and the primary control systems. Since the weight penalty imposed by the vibration control system is determined largely by the actuator system, the increase in blade pitch-link loads should be kept to a minimum. The influence of blade torsion frequency on the pitch-link loads and the actuator power requirement for HHC is also examined. This parametric study is prompted by the results of Ref. 10, which showed that the blade torsion frequency placement had a significant effect on the stall flutter behavior of rotors. For some rotor designs, the flight envelope is limited by control load saturation caused by stall flutter.

The analytical study uses a comprehensive, coupled aeroelastic analysis developed at the Rotorcraft Center, University of Maryland. The analysis employs state-of-the-art modeling techniques, which include a finite element method in both space and time domain, a modern unsteady aerodynamic model that incorporates dynamic stall effects (Leishman's model), and the comprehensive analytical model of rotor aerodynamics and dynamics (CAMRAD) nonuniform inflow models. Several correlation studies have been carried out to validate the analysis, and typical results can be found in Ref. 11. Excellent correlation of the calculated vibratory hub loads with Boeing wind-tunnel data[12] has been obtained with the refined aerodynamic modelings. However, due to the lack of HHC experimental data, this analysis was not validated with HHC results, and as such, the results presented herein should be interpreted with some degree of caution.

Formulation

Elastic Blade Model

In the analysis, the rotor blade is modeled as an elastic beam, undergoing flap bending, lead-lag bending, torsion, and axial deflections. The finite element method based on Hamilton's principle is used to discretize the blade into a number of beam elements, each with 15 degrees of freedom. Between elements, there is continuity of displacement and slope for flap and lag bending deflections and continuity of displacement for elastic twist and axial deflection. The formulation is developed for a nonuniform blade having pretwist, precone, and chordwise offsets from the blade pitch axis for blade center of mass, aerodynamic center, tensile axis, and elastic axis.

Blade Air Loads and Rotor Inflow

The aerodynamic loading is calculated using a nonlinear unsteady aerodynamic model based on the works of Leishman and Beddoes.[13] This model consists of an attached compressible flow (linear) formulation along with a representation of the nonlinear effects due to flow separation and dynamic stall.

For steady inflow calculation, wake models adapted from the government rotor code CAMRAD[14] are used. In particular, two nonuniform inflow models are utilized in this study: Langrebe's prescribed wake model for the low-speed regime, and a free wake model for the high-speed cases.

Vehicle Trim and Blade Response

In the analysis, the vehicle trim control settings and the blade steady responses are calculated iteratively as one coupled solution. For a free flight condition, the vehicle equilibrium equations consist of three force and three moment equations in the body-fixed axis system. For a wind-tunnel condition, the rotor shaft orientation is fixed and the rotor is trimmed for a prescribed thrust and steady hub moments or cyclic flapping angles.

For a given set of trim controls, the blade steady response for one rotor revolution is calculated. Using finite element discretization, the blade governing equations are obtained as a set of nonlinear, ordinary differential equations with periodic coefficients. Then, a modal reduction technique is applied, resulting in a set of normal mode equations that are solved using a finite element method in time. Using a modified Newton method, the trim control settings are updated based on the vehicle equilibrium condition. The process of calculating blade steady responses and updating trim controls is repeated until the overall solution converges. The converged solutions satisfy simultaneously the overall vehicle steady force and moment equations for a prescribed flight condition.

Higher Harmonic Control System

A linear frequency-domain model in the form of a transfer matrix is adopted to relate the harmonics of HHC inputs to the harmonics of the vibratory hub loads.[11] A closed-loop controller is used in this analysis, and the HHC model is

$$z_n = z_{n-1} + T_n(\theta_n - \theta_{n-1}) \tag{1}$$

For vibratory hub shear suppression, the response vector z_n has 10 components and consists of sine and cosine harmonics of the vibratory hub loads (vertical, longitudinal, and lateral hub shears along with pitching and rolling moments); the input vector θ has six components and consists of sine and cosine harmonics of the higher harmonic blade pitch at three distinct frequencies of $(N-1)P$, NP, and $(N+1)P$; T_n is the transfer matrix; and the index n denotes the current HHC cycle. In the analysis, an HHC cycle corresponds to a rotor revolution.

For rotor performance improvement, z_n represents the rotor shaft torque and is simply a scalar; θ is a vector with two components, θ_{2c} and θ_{2s}; T_n, in this case, is a row vector with two components. Note that for this case, only the 2P component is used in order to minimize the effects of HHC inputs on vibration. Furthermore, the 2P blade pitch amplitude is constrained at a predetermined angle. This constraint is introduced to avoid control divergence and reflects an actual actuator hardware limit.

For vibratory hub shear suppression and rotor performance improvement, optimal control is obtained by minimizing the quadratic performance index J

$$\min J = \min\left(\frac{1}{2} z_n^T W_z z_n + \frac{1}{2} \Delta\theta_n^T W_{\Delta\theta} \Delta\theta\right) \tag{2}$$

where W_z and $W_{\Delta\theta}$ are weighting matrices for z and θ, respectively, and $\Delta\theta_n = \theta_n - \theta_{n-1}$. The corresponding optimal control is

$$\theta_n = \theta_{n-1} + (1-r) C_n z_{n-1} \tag{3}$$

where

$$C_n = -(T_n^T W_z T_n + W_{\Delta\theta})^{-1} T_n^T W_z \tag{4}$$

and r is the control rate limiting factor with values ranging from 0.0 to <1.0. The factor $(1-r)$ is introduced to constrain the HHC control rate and help reduce large control excursions. This is useful from the actuator response standpoint, and a suitable value of r can be used to stabilize the feedback system. Note that, for performance improvement, the results

of Eq. (4) are used to determine the optimal phase angle only because the control amplitude is fixed.

For the first HHC cycle, the transfer matrix is generated using a finite difference approach. For this, each component of the HHC vector is activated by generating a sequence of perturbed z responses about the uncontrolled value. Then each column of T_o is the ratio of the difference between the perturbed and unperturbed response vectors and the perturbed HHC inputs. For subsequent HHC cycles, the transfer matrix is updated using the secant method.[11]

For a given actuator size and pitch-link configuration, the actuator power can be expressed in terms of an actuator power index defined as[12]

$$S_n = \sqrt{(C_{\text{col},c} + C_{\text{lat},c})^2 + (C_{\text{col},s} + C_{\text{lat},s})^2} + \sqrt{(C_{\text{col},c} - C_{\text{lat},c})^2 + (C_{\text{col},s} - C_{\text{lat},s})^2} + \sqrt{(C_{\text{col},c} + C_{\text{long},c})^2 + (C_{\text{col},s} + C_{\text{long},s})^2} + \sqrt{(C_{\text{col},c} - C_{\text{long},c})^2 + (C_{\text{col},s} - C_{\text{long},s})^2} \quad (5)$$

where $C_{(.)}$ are the higher harmonic swash-plate motions; the subscripts col, long, and lat refer, respectively, to the higher harmonic collective, longitudinal, and lateral modes; and the subscripts c and s refer to the cosine and sine harmonics, respectively. These swash-plate motions are derived from the higher harmonic blade pitches with a linear transformation derived from the control system geometry. In this form, the actuator power index represents a collective measurement of the blade HHC amplitudes.

Results and Discussion

In this study, a three-bladed articulated rotor is used. The rotor properties are modeled after the CH-47D scaled model rotor, which was wind-tunnel tested by Boeing Helicopter Company in their HHC program.[8] The general rotor characteristics are presented in Table 1, and a further detailed description of the blade properties can be found in Ref. 11. The rotor is simulated for the wind-tunnel conditions, and the calculated trim controls correspond to a specified thrust, advance ratio, and a shaft tilt angles. For this wind-tunnel simulation, the cyclic flapping angles at the blade hinge are trimmed to zero.

Correlation to Rotor Shaft Power

The analysis is validated by a correlation of the predicted rotor shaft power with experimental data, as shown in Fig. 1. The results are shown for forward speeds from hover to 160 kt at a constant blade thrust level ($C_T/\sigma = 0.08$, where C_T is the rotor thrust coefficient, and σ is the rotor solidity ratio). Furthermore, the results are expressed in terms of the shaft power coefficient weighted by the solidity ratio (C_p/σ). The overall correlation is fair, and the calculated results consistently underpredict the rotor shaft power for the whole speed range. Except for the results near 40 kt where the discrepancies are large, this analysis underpredicts the experimental results by up to 10%. This discrepancy is attributed to the Reynolds number effects associated with the scaled model rotor.

Table 1 Blade and rotor properties

Blade number	3
Blade radius, R	5.23 ft
Flap hinge offset	0.0286 R
Rotor rotational speed, rpm	1333.6
Rotor solidity ratio, σ	0.0711
Blade linear pretwist	−14 deg
Blade natural frequencies, per rev	
Rigid lag	0.50
Rigid flap	1.023
First elastic flap	2.66
Rigid torsion	4.86
Second elastic flap	5.21
First elastic lag	6.39
Third elastic flap	8.92
First elastic torsion	11.44

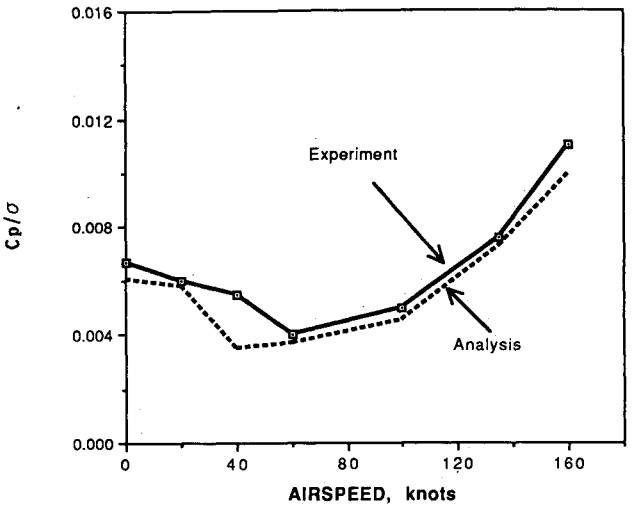

Fig. 1 Correlation of predicted rotor shaft power with wind-tunnel data[8] ($C_T/\sigma = 0.08$).

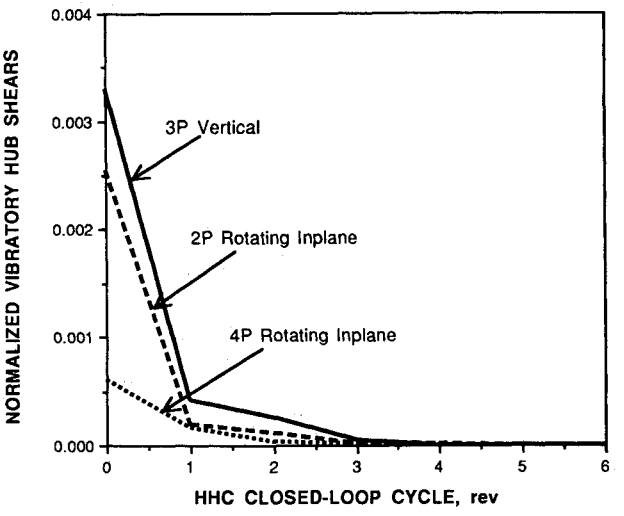

Fig. 2 Vibratory hub shear responses with HHC ($\mu = 0.3$, $C_T/\sigma = 0.09$).

Higher-Harmonic-Control-Induced Blade Stall

The flight condition of 135 kt ($\mu = 0.3$) and $C_T/\sigma = 0.09$ was chosen to investigate the effects of HHC on blade stall. For this, the global controller (with $r = 0$) was used to suppress all three vibratory hub shears. The vibratory hub shear responses, presented in Fig. 2, indicate that all three hub shear components are completely suppressed within three cycles. The blade section normal force coefficient computed at 93% blade radius for the cases with and without HHC are shown in Figs. 3 and 4, respectively. In these figures, C'_N is the substitute normal force coefficient that includes shed wake and stall delay effects, C_N is the total normal force coefficient that includes both nonlinear trailing-edge separation and dynamic stall effects, and the stall boundary is the critical normal force value C_{N1}. In the aerodynamic formulation, dynamic stall is initiated when the value of C'_N exceeds the critical normal force value, and a stall margin is defined as the difference between C'_N and C_{N1}. Figure 3 shows that, without HHC, the stall margin value for this particular blade section is about 0.4–0.5 for the complete range of the rotor azimuth.

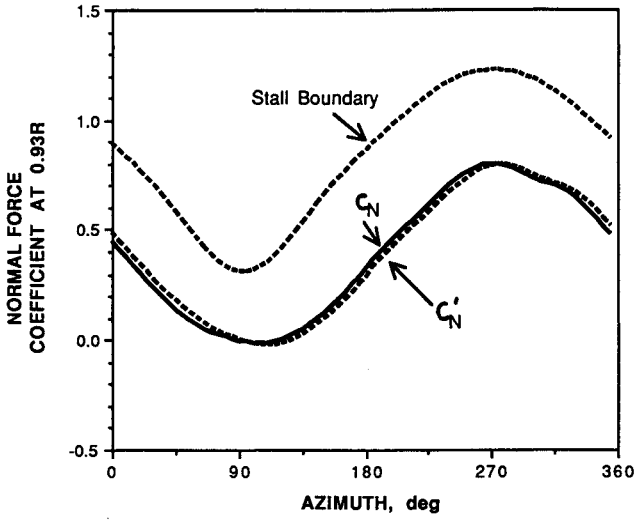

Fig. 3 Normal force coefficient waveform at 0.93 blade radius with HHC off (μ = 0.3, C_T/σ = 0.09).

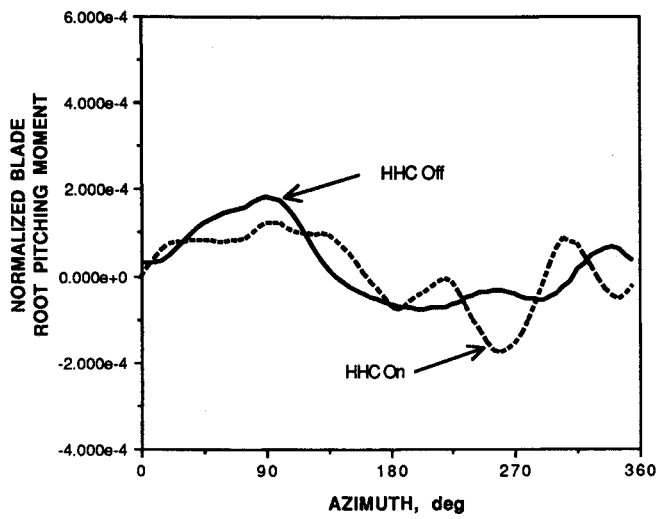

Fig. 6 Effects of HHC on blade root pitching moment (μ = 0.3, C_T/σ = 0.09).

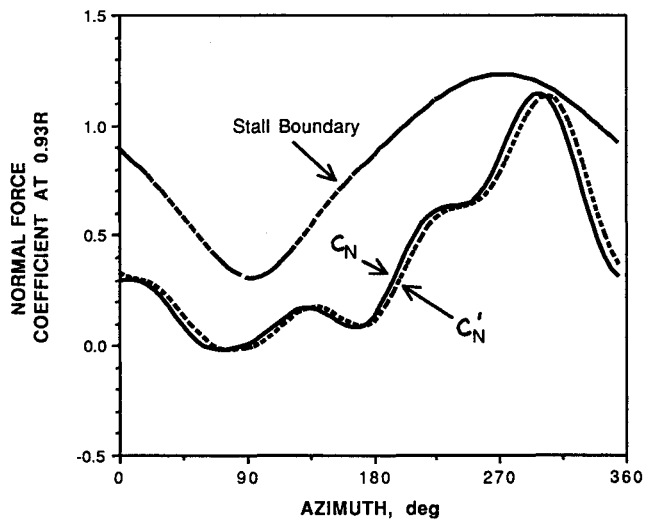

Fig. 4 Normal force coefficient waveform at 0.93 blade radius with HHC on (μ = 0.3, C_T/σ = 0.09).

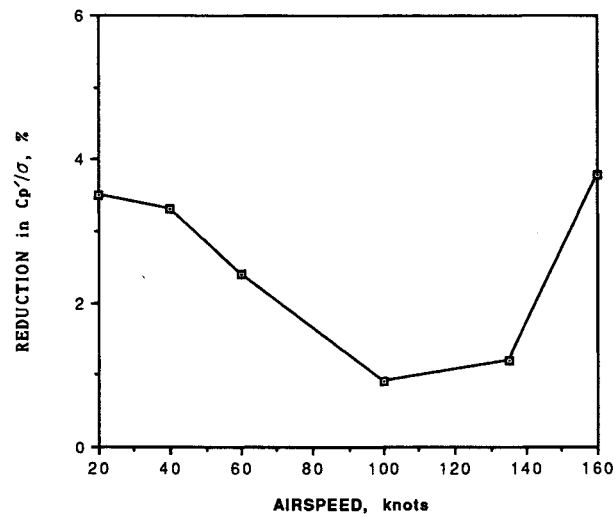

Fig. 7 Rotor performance improvement with 2/rev blade pitch control (C_T/σ = 0.08).

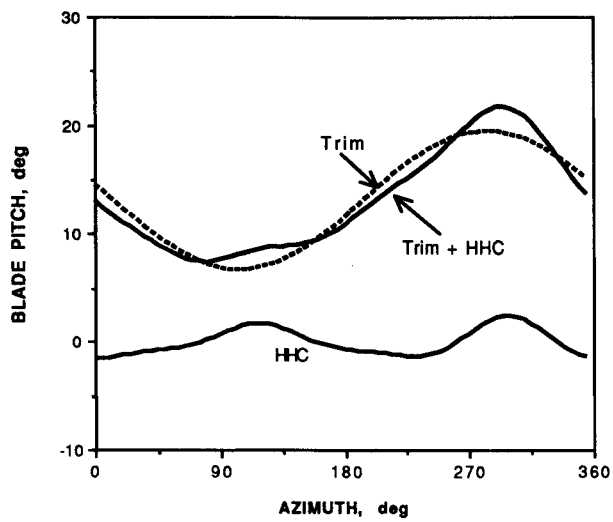

Fig. 5 Comparison of blade trim and HHC pitches (μ = 0.3, C_T/σ = 0.09).

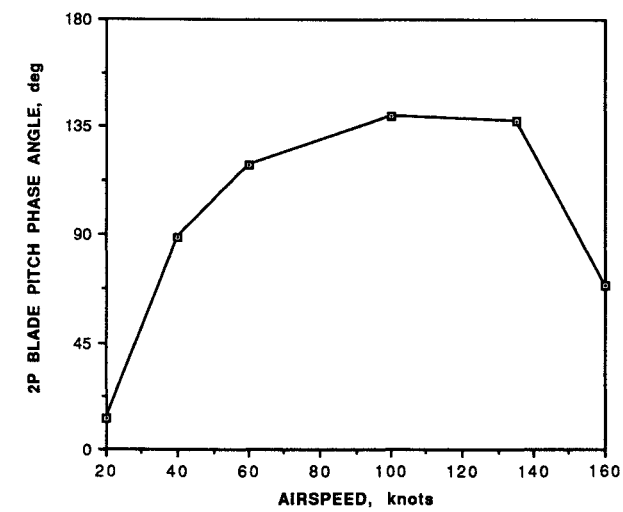

Fig. 8 Phase angle of 2/rev blade pitch control for rotor performance improvement (C_T/σ = 0.08).

However, with HHC on, Fig. 4 shows that the stall margin for this particular blade section is reduced to <0.1 in the fourth quadrant of the rotor disk.

The blade trim and HHC input waveforms are shown in Fig. 5. The HHC waveform is nose up side to side and is dominated by the 2*P* component. By comparing the blade pitch with trim only and with trim plus HHC, it can be seen that the basic blade pitch is increased (nose up) due to the HHC component by more than 2 deg on the retreating side, which could mean blade stall. A smaller increase is also noted in the advancing side, from 85 to 150 deg of rotor azimuth.

As another indication of stall, Fig. 6 shows the effects of HHC on the blade root pitching moment. The effects of HHC on the advancing side are quite favorable, i.e., the pitching moment is reduced with HHC. The effects are reversed on the retreating side. The large nose down pitching moment around 270 deg azimuth, with HHC on, is a clear indication of blade stall. The subsequent pitching moment response in the fourth quadrant of the rotor disk, manifested by a secondary sharp nose down followed by a sharp nose up pitching moment, is a typical stall flutter behavior. These results all show that HHC inputs used for vibratory hub shear suppression may promote blade stall.

Performance Improvement with Higher Harmonic Control

The effects of HHC, when the controller is configured to improve rotor performance, are examined next. In this simulation, the flight conditions and the rotor model are identical to those used in the shaft power correlation study. For these results, the 2*P* blade pitch amplitude is set to 2 deg. Furthermore, the HHC inputs are constrained by setting $W_{\Delta\theta} = \varepsilon I_2$, where ε is a small number varying from 0.35×10^{-6} to 1.0×10^{-6}, and I_2 is the 2×2 identity matrix. This constraint is introduced to avoid the singularity of the matrix $(T_n^T W_z T_n + W_{\Delta\theta})$, which appears in Eq. (4). The performance gain with HHC is presented in Fig. 7 for forward speeds from 20 to 160 kt. Since the rotor is not retrimmed after application of HHC, the 2*P* control induces small changes to the rotor propulsive force and negligible changes to the rotor thrust. To reflect the change in propulsive force, the results are presented in terms of a rotor power coefficient C_p'/σ, defined as the difference between the total rotor shaft power coefficient and the parasite power coefficient. In particular, the rotor power consists of the rotor induced power and profile power. Note that the parasite power is the power required to sustain a propulsive force and is equal to the product of the propulsive force and the forward speed. Within the range of speed down, the largest gain in performance occurs at 160 kt with almost 4% reduction in the rotor power. The smallest gain in rotor performance occurs at 100 kt with <1% reduction in rotor power.

The 2*P* control phase variation with forward speed is presented in Fig. 8. The results indicate that, near a hover flight condition (20 kt), the improvement in rotor performance is achieved with the maximum blade pitch amplitude at the fore and aft regions of the rotor disk. As the forward speed is increased to 60 kt, the 2*P* control peaks shift toward the advancing and retreating sides. This 2*P* control phase angle remains constant at approximately 125 deg for speeds ranging from 60 to 135 kt and drops sharply as the forward speed is increased further. In particular, the higher harmonic blade pitch at 160 kt peaks at 35 and 215 deg azimuth.

Figure 9 shows the blade lift coefficient waveform, with HHC on and off, at the three-quarter blade radius for the flight condition at 160 kt. For this flight condition, the net effect of the optimum 2*P* blade pitch is to increase the lift components in the first and third quadrants of the rotor disk while decreasing lift in the other two quadrants. The same trend in lift redistribution, with small phase shift, is also observed at all other flight conditions simulated. Note that the change in lift distribution is due primarily to the combined effects of the changes in blade pitch, blade flapping, elastic twist, and the shed and trailed vorticities.

The 2*P* control used to improve rotor performance significantly increase the 2*P* rotating in-plane hub shear for the complete speed range. This adverse effect is presented in Fig.

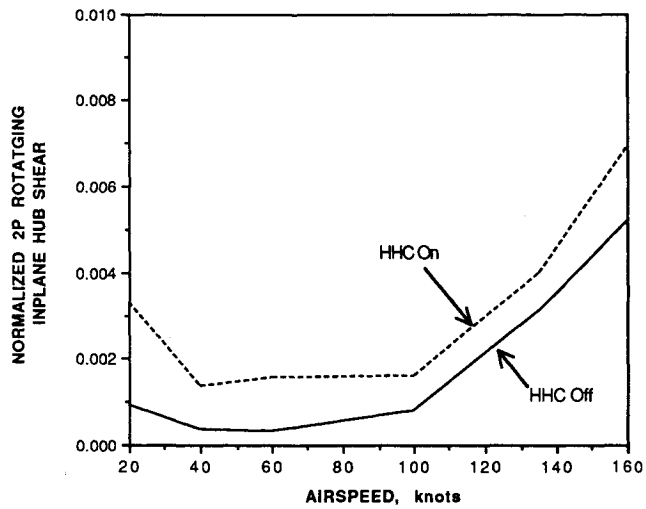

Fig. 10 Effects of 2/rev blade pitch control for rotor performance on 2/rev rotating in-plane hub shear ($C_T/\sigma = 0.08$).

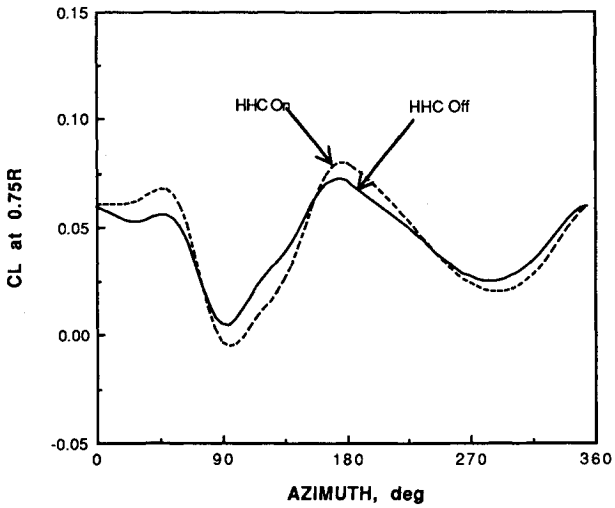

Fig. 9 Normal force coefficient waveform at 0.75 blade radius with and without 2/rev blade pitch control ($\mu = 0.35$, $C_T/\sigma = 0.08$).

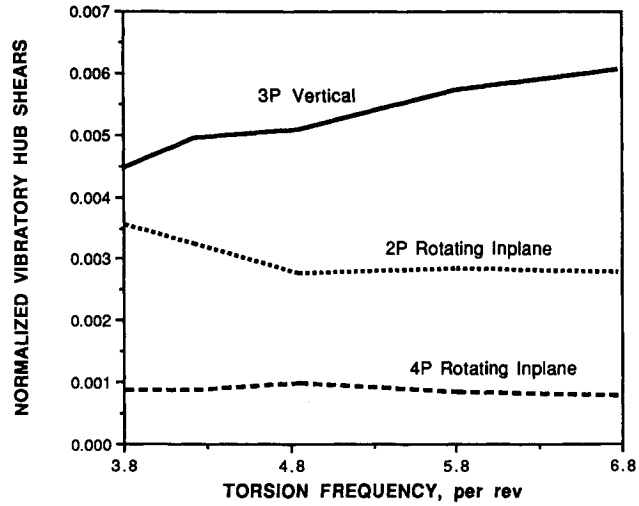

Fig. 11 Effects of blade torsion stiffness on the uncontrolled vibratory hub shears ($\mu = 0.3$, $C_T/\sigma = 0.12$).

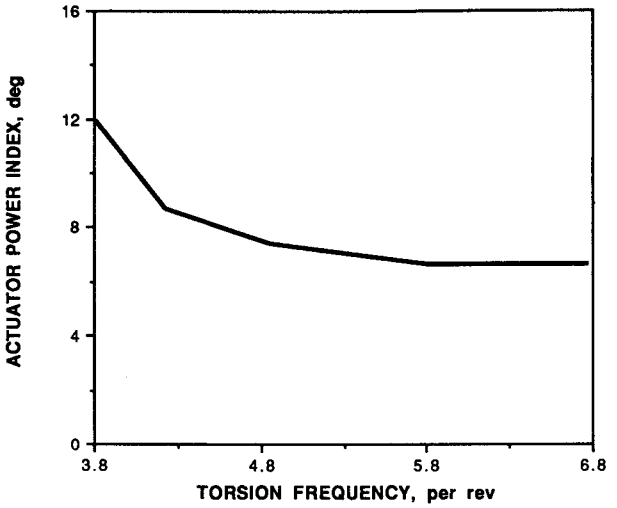

Fig. 12 Effects of blade torsion stiffness on the actuator power index (μ = 0.3, C_T/σ = 0.12).

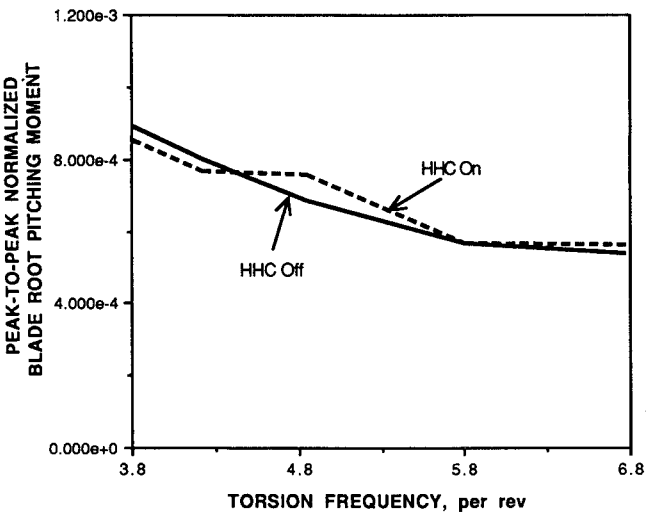

Fig. 13 Effects of blade torsion stiffness on the peak-to-peak blade root pitching moment (μ = 0.3, C_T/σ = 0.12).

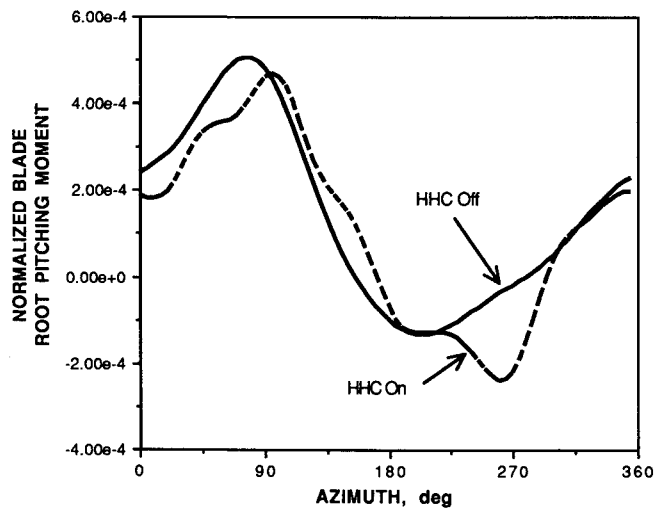

Fig. 14 Effects of HHC on blade root pitching moment (μ = 0.3, C_T/σ = 0.12, v_ϕ = 4.86).

10, which shows that the largest increase in $2P$ in-plane hub shear occurs at both high-speed regime and hover. The $3P$ vertical and the $4P$ rotating in-plane hub shears are also affected, but the net effects are much smaller and can be neglected. For a three-bladed rotor, the $2P$ inplane blade shears are summed at the hub and transmitted to the airframe, causing $3P$ in-plane vibration.

Effects of Blade Torsion Stiffness

Effects of blade torsion stiffness on the vibratory hub shears, pitch-link loads, and actuator power required for vibration suppression are examined next. In this simulation, the blade fundamental (rigid mode) torsion frequency varies from 3.8 to $6.8P$, where the baseline value is $4.86P$. The flight condition is 135 kt (μ = 0.3) and C_T/σ = 0.12.

The HHC controller based on the local model is used to suppress the $3P$ vertical and the 2 and $4P$ rotating in-plane hub shears. The results for the vibratory hub shears with HHC are not shown because, for the cases presented, they are suppressed by more than 95% from the uncontrolled values. For the configurations when the blade torsion frequencies are $<3.8P$, the HHC input requirements are so large that numerically converged solutions cannot be obtained.

Figure 11 shows the influence of the blade torsion frequencies on the vibratory hub shears with HHC off. For most of the frequency range, the in-plane hub shears are quite insensitive to the blade torsion stiffness. When the blade torsion frequency is below the baseline value, the $2P$ in-plane component increases slightly, whereas the $4P$ component decreases slightly from the baseline blade configuration. Such variations in the in-plane hub shears are probably due to the coupling between the in-plane and the out-of-plane loadings, which exists for soft torsion blades. On the other hand, the $3P$ vertical hub shear increases moderately with increase in the blade pitch-link stiffness. In fact, the $3P$ vertical component increases by a third as the blade torsion frequency is increased from 3.8 to $6.8P$.

The variation of the actuator power index, Eq. (5), with the fundamental blade torsion frequency is shown in Fig. 12. This figure shows that a stiff torsion blade with a frequency $>4.5P$ requires about 40% less HHC amplitude than a soft torsion blade with a frequency equal to $3.8P$. For torsion frequencies $>5.8P$, the HHC amplitudes are not sensitive to the control stiffness.

Figure 13 shows the peak-to-peak blade root pitching moment, a direct measurement of the blade pitch-link and control system loads. In the figure, results with HHC both off and on are presented. The results with HHC off show that the pitching moment decreases with increasing torsion frequency. With HHC on, the pitching moment first decreases for the range of torsion frequency from 3.8 to $4.2P$, increases slightly for frequencies from 4.2 to $4.86P$, and decreases again for higher torsion frequencies. The changes in blade pitching moment due to HHC are small and remain within 10% of the uncontrolled values. Since the actuator power is proportional to the product of the actuator power index and the control load, these results indicate that a torsionally stiff blade requires significantly less actuator power than a torsionally soft blade for the flight condition considered.

The effects of HHC on the blade pitching moment waveform are shown in Fig. 14, and the results are shown only for the baseline blade configuration (with a torsion frequency equal to $4.86P$). This figure shows that the large increase in nose down pitching moment on the retreating side, due to the HHC induced stall, is compensated by a smaller reduction on the advancing side. The resulting effect is a relatively smaller net increase in the peak-to-peak value.

Conclusions

An advanced higher harmonic control analysis has been used to investigate HHC effectiveness in vibratory hub shear suppression and basic rotor performance enhancement. Re-

sults from a correlation study indicate that the prediction of the rotor total power is fair. The following conclusions have been drawn from this study.

1) 2/rev blade pitch control is capable of improving rotor aerodynamic efficiency. Reduction up to 3.8% in rotor power is achievable with 2 deg of $2P$ blade pitch. Improvement in performance was obtained at the expense of increased vibratory hub shears.

2) For moderately high speed and high thrust flight ($\mu = 0.3$, $C_T/\sigma = 0.09$), HHC used for vibratory hub shear suppression promotes stall on the retreating side of the rotor disk.

3) Effects of blade torsion frequency on the vibratory hub shears and HHC performance are moderate at high thrust and moderately high-speed regime ($\mu = 0.3$, $C_T/\sigma = 0.12$). The peak-to-peak blade pitch-link loads do not change significantly with blade torsion frequency. The actuator power required to suppress the vibratory hub shears for a stiff torsion blade is significantly lower than that for a soft torsion blade.

References

[1]Wood, E. R., Powers, R. W., Cline, C. H., and Hammond, C. E., "On Developing and Flight Testing a Higher Harmonic Control System," *Journal of the American Helicopter Society*, Vol. 30, No. 1, 1985, pp. 3–20.

[2]Miao, W., Kottapali, S. B. R., and Frye, H. M., "Flight Demonstration of Higher Harmonic Control (HHC) on S-76," *Proceedings of the 42nd Annual National Forum of the American Helicopter Society*, American Helicopter Society, Alexandria, VA, 1986.

[3]Polychroniadis, M., and Achache, M., "Higher Harmonic Control: Flight Tests of an Experimental System on SA 349 Research Gazelle," *Proceeedings of the 42nd Annual National Forum of the American Helicopter Society*, American Helicopter Society, Alexandria, VA, 1986.

[4]Stewart, W., "Second Harmonic Control in the Helicopter Rotor," Aeronautical Research Council, RM-2997, London, Aug. 1952.

[5]Payne, P. R., "Higher Harmonic Rotor Control," *Aircraft Engineering*, Vol. 30, No. 354, Aug. 1958, pp. 222–226.

[6]Arcidiacono, P. J., "Theoretical Performance of Helicopters Having Second and Higher Harmonic Feathering Control," *Journal of the American Helicopter Society*, Vol. 6, No. 2, 1961, p. 8–19.

[7]Drees, J. M., and Wernicke, R. K., "An Experimental Investigation of a Second Harmonic Feathering Device on the UH-1A Helicopter," United States Army Transportation Research Command, TR-62-109, Fort Eustis, VA, June 1963.

[8]Shaw, J., Albion, N., Hanker, E. J., and Teal, R. S., "Higher Harmonic Control: Wind Tunnel Demonstration of Fully Effective Vibratory Hub Forces Suppression," *Journal of the American Helicopter Society*, Vol. 34, No. 1, 1989, pp. 14–25.

[9]Polychroniadis, M., "Generalized Higher Harmonic Control, Ten Year of Aerospatiale Experience," *Proceedings of the 16th European Rotorcraft and Vertical Lift Conference*, Glasgow, Scotland, UK, Sept. 1990.

[10]Tarzanin, F. J., and Ranieri, J., "Investigation of the Effect of Torsional Natural Frequency on Stall Induced Dynamic Loading," United States Army Air Mobility Research and Development Laboratory, TR-73-94, Fort Eustis, VA, Feb. 1974.

[11]Nguyen, K., and Chopra, I., "Application of Higher Harmonic Control to Rotors Operating at High Speed and Thrust," *Proceedings of the 42nd Annual National Forum of the American Helicopter Society*, American Helicopter Society, Alexandria, VA, 1989; also, *Journal of the American Helicopter Society*, Vol. 35, No. 3, 1990, pp. 78–89.

[12]Nguyen, K., and Chopra, I., "Application of Higher Harmonic Control (HHC) to Hingeless Rotor System," *Proceedings of the 30th AIAA Structures, Structural Dynamics, and Materials Conference*, AIAA, Washington, DC, April 1989.

[13]Leishman, J. G., and Beddoes, T. S., "A Semi-Empirical Model for Dynamic Stall," *Journal of the American Helicopter Society*, Vol. 34, No. 3, 1989, pp. 3–17.

[14]Johnson, W., "A Comprehensive Analytical Model of Rotor Aerodynamics and Dynamics, Part I: Analysis and Development," NASA TM-81182, June 1980.